

An assessment on effect of process parameters on pull force during pultrusion.

MUKHERJI, A. and NJUGUNA, J.

2022

© The Author(s) 2022.



An assessment on effect of process parameters on pull force during pultrusion

Arindam Mukherji^{1,2} · James Njuguna^{2,3}

Received: 9 July 2021 / Accepted: 12 April 2022 / Published online: 22 June 2022
© The Author(s) 2022

Abstract

This research investigates the process behaviour by prediction of the pull force required to drag the raw materials through heated die at different reinforcing material configuration during pultrusion. Pultrusion is a continuous manufacturing process that is widely used in manufacture for composite profiles. A specially designed device, friction force by virtue of pulling on ‘resin impregnated’ fibres with both liquid resin and partially cured resin, was employed to measure pulling force against temperature and resin conversion. This allowed to experimentally simulate materials tracing in short and long die length used in process. Differential scanning calorimetry (DSC) was used to determining polymer conversion. The results shows that the downstream part of a die has no significant effect on the pulling force before a specific conversion level is achieved and that higher resin conversion leads to a higher friction at viscous/liquid zone. The difference noted is much more significant when the temperature is low (e.g. room temperature) and considerably drops due to on rising temperature. Further, a new mathematical model is proposed that predicts the rise in compaction pressure on increasing fibre volume fraction and drag velocity which is an opposite characteristic to tapping angle and part thickness considerations. Similarly, many parameters including shrinkage, viscous force and dry friction were modelled and simulated for ortho polyester resins as a function of temperature and resin conversion during dynamic pulling. The study has direct application in configuring pultrusion manufacturing customisation for a specific configured material, components manufacturing and respective designing of the die for the profile to be manufactured.

Keywords Pultrusion · Modelling · Die · Polyester · Curing · Compaction force · Viscous force · Frictional force · Drag velocity

1 Introduction

The pulling of wet reinforcing fibres through die may be simple; however, the dynamics and mechanisms of process parameters are very complex to fully comprehend due to continuous interaction between physical and chemical changes. In the literature, numerical and experimental investigations were attempted by several researchers to predict

aspects of intrinsic pultrusion process to evaluate, e.g. pressure [1–5], cure mechanism [6, 7], pull force [8–10] and heat transfer mechanism. Phenomena involved are mainly heat transfer controlling viscosity of the resin, resin conversion and phase changes, die-material/surface in contact and stress–strain behaviour. To model pultrusion process focusing on pull forces, it is recommended that the material inside should be divided into separate regions such as taper region at wet material entry side, thermally active gel where process of curing is initiated, post gel region and region of separation region or part detached from die surface.

A statistical investigation on influence of process parameters like pull force and flexural strength of pultruded product was made by Lackey and Vaughan [11] and it was concluded that process parameters, influences pulling force, may vary significantly due to complex interaction change in cure kinetics [12, 13]. On the other hand, to have satisfactory experimental analysis, the elevated

✉ James Njuguna
j.njuguna@rgu.ac.uk

¹ SP Advance Engineering Materials Pvt Ltd, SP Centre, Minoo Desai Marg, 41/44, Colaba, Mumbai 400 005, India

² Advanced Materials Research Group, School of Engineering, Robert Gordon University, Garthdee Road, Aberdeen AB10 7GJ, UK

³ National Subsea Centre, AB21 0BH Aberdeen, United Kingdom

number of variables involved which are to consider is an undesirable time consuming and money spending operation. Even prediction of part properties from process intricacy is barely perceptible. For any explicit understanding of pultrusion operation, mathematical modelling should embrace fundamental laws for heat transfer, conservation of mass and momentum. For simplification, very few aspects have been studied in the literature when deriving numerical solution.

The process involves complex effect on cure kinetics resin, permeability, porosity and shape factor of roving of reinforcing materials. The permeability of any porous material was first investigated and proposed by Henry Darcy widely known as Darcy's law. Change in pressure gradients during flow for hydraulic fluid depends on conductivity of the fluid involved wherein permeability and porosity controls pressure gradient for porous materials like resin impregnated fibres for thermoset and thermoplastics materials.

$$v = -K/\eta \nabla P \quad (1)$$

In the expression, v is the velocity of drag or pulling, K is permeability and ∇P is pressure difference and η is viscosity of resin. In Kozeny-Carman equation of permeability, where a model for ellipsoid material with granular beds was assumed to be valid for fibrous porous media [14, 15] is widely used.

$$K = R^2/(4k_c) * [(1 - V_f)^3/V_f^2] \quad (2)$$

where k_c is the Kozeny constant, R the particle radius and V_f the fibre volume fraction.

Gutowski et al. [16, 17] analysed compressibility and permeability of carbon fibre stack impregnated with oil as follows

$$P = \frac{3\pi B(\sqrt{(V_f/V_0)} - 1)}{[\beta^4(\sqrt{(V_a/V_f)} - 1)^4]} \quad (3)$$

In the proposed mathematical expression, P is pressure normal to surface as given in Eq. (3). The transversal stiffness of fibres B and β is the constant representing ratio of span length to span height of the fibres involved. V_f final fibre volume fraction of the product wherein V_0 and V_a initial fibre volume and maximum fibre volume fraction reconsidered in the model. This expression indicate that only pressure is being experienced by fibres packs.

In conventional pultrusion or in open bath pultrusion, compaction force or the pressure arises due to compaction is ignored due to low fibre volume fraction and short taper length. But with reasonable tape length in open bath pultrusion, increased fibre volume can be achieved without

injection pressure [18–21]. Complexity of viscous region and compaction zone is profound for fast curing resin like polyester. Hence, to maintain higher tapping and viscous length die, specific design is required to be adopted.

The analytical model of Kim et al. [22, 23] proposes pressure inside pultrusion die as unidirectional flow in pulling direction and no permeability in z-direction. The expression is normally used for matrix continuity model.

$$dP/dx = U * \eta/K_{(x)} * [1 - V_{fx} - (1 - \Delta v/v) * (V_{fx}/V_f - V_{f(x)})] \quad (4)$$

In this Eq. (4), U is the pulling speed, (x) is the longitudinal permeability and V_{fx} is the fibre volume fraction as functions of axial distance. $\Delta v/v$ represents the resin resultant volume change due to thermal expansion and overall shrinkage which can be ignored for simplification. Interactive pressure of respective regions can be calculated by integrating this expression with elemental respective axial distance is expressed in Eq. (5).

$$P(x) = U * \eta/K(x) * [1 - V_{fx}/V_f] * x \quad (5)$$

However, many researchers proposed injection pultrusion, and total pulling force contribution is calculated as $F_{tot} = F_{com} + F_{vis} + F_{fric}$, where F_{tot} is total pulling force, F_{com} is compaction force and F_{fric} is frictional for after separation. These three different resistances are expressed separately by considering die width 'w' and axial distance:

$$F_{com} == \int 2w(\dot{p} + \sigma)\tan\theta dx \quad (6)$$

$$F_{vis} == \int 2w\tau dx \quad (7)$$

and

$$F_{fric} == \int 2wf.\sigma dx \quad (8)$$

within $0 \leq x \leq x_{in}$.

Pull-force modelling for other injection pultrusion indicates that several factors like sliding-induced shear and viscous adhesion force shrink-induced part-detached play's important role are unaccounted on analytical models. In Eq. (5) for compaction, Eq. (6) for viscous drag force and Eq. (8) of friction coefficient have neither considered thin layer resin at die composite interface for zones separately for compaction zone, liquid zones and dry profile zones beyond curing nor the thermal expansion and shrinkage. Even bending angle of reinforcing fibres as function of axial length in taper section which plays a major role in controlling pull force is not conserved. Bending angle depends on the

stiffness of the fibres and the length of the taper section die eventually compaction angle.

This work efforts are to capture complex variables like normal force, resin conversion, line speed and temperature by modifying many existing parameters during scale-up operation. Pressure-dependant variables are used in the proposed model to predict the experimental results at operation. In this study, experimental quantification on pull force in compaction die is performed on conventional pultrusion dies of two different tapping angles, wherein effect of temperature and fillers on straight die on friction is being testified by results received from inhouse made device. Along with polymer thin layer conversions separately for differ zones, flat straight die profile, thermal expansion and shrinkage, this mathematical model manifested the effects of die-compaction angle, fibre volume fraction, thickness and drag velocity on pull force. Therefore, the aim of this paper is to evaluate the effect of process parameters on pull force configuring materials and designing of die for the profile to be pultruded.

2 Experiments

2.1 Materials

A continuous random glass fibre mats with 450 and 300 g/m² (gsm) were provided by Skaps Industries India PVT Ltd. Owens Corning supplied glass roving used was of 4800 tex (tex: the mass in gram per one kilometre of a fibre roving). A concoction of random glass mats and glass roving fibre package of 600 gsm were used. Organically modified montmorillonite (MMT) was obtained from SIGMA–ALDRICH. The OMMT contained 0.05–5 wt% aminopropyltriethoxysilane and 15–35 wt% of ocatadecylamine, appearance (colour) white to off-white appearance (form) powder, loss on drying $\leq 3.0\%$, size ≤ 20 -micron and density 200–500 kg/m³ (bulk density). Precipitated calcium carbonate (CaCO₃) powder from Gulshan Polyols Limited was employed as the conventional micron-filler of size ≤ 40 -micron particle size. Orthophthalic acid-based unsaturated polyester resin (MECH-STER™ 9000P) tailored for the pultrusion process and supplied by Mechamco Resins Ltd was used in this study.

2.2 Characterisation

Differential scanning calorimetry (DSC) experiments were performed on a TA-60 Plus Shimadzu instrument, using hermetic pans and sample weights lower than 10 mg. The used materials in the experiments are formulated in resin paste and different low conversion as mentioned in Tables 1 and 2.

Isothermal scans were run at temperatures typically around 80 °C and kept it for 30 min to run out the residual Initiators. All curatives and additives are premixed

Table 1 Materials and formulation used for the friction measurement

Ortho-polyester resin	Mechemco	100 phr
Perkadox-C	Ackzonoble	0.050 phr
MEKP	Aldrich chemical	0.25–0.50 phr
BPO	Veekay chemicals	1.0 phr
TBPB	Veekay chemicals	1.2 phr
Calcium carbonate-400	GULSHAN Polyols limited	30 pbw
Release oil	Fine organics	1 pbw

separately before sampling. The sample preparation was done swiftly in order to avoid the loss of volatiles such as styrene that results in loss of data during the first stages of the reaction. DSC determines the conversion of resin by measuring residual heat by thermal initiation. Table 2 shows the final conversion and curatives like Paradox-C, MEKP, BPO and TBPB used in the experiment.

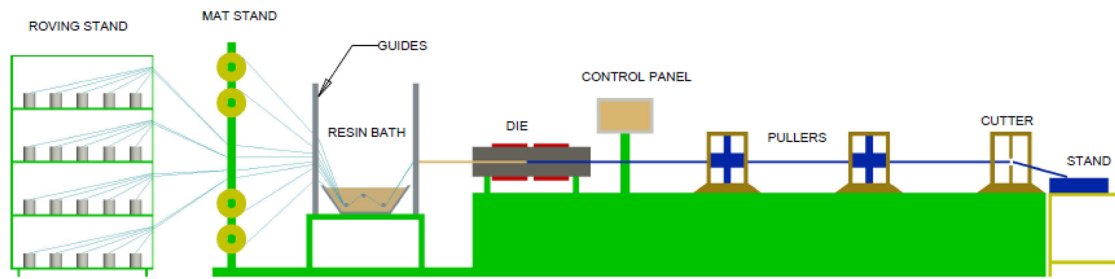
2.3 Pultrusion line and experiment set up

Working line schematic used in our work is shown in Fig. 1a. The line consists of creel stands for roving and racks for felts, veil fabrics and unwinding continuous filament-mat (CFM), a resin tank, a pre-forming assembly composed of perforated steel plates and other guide rollers, and a heated die, die with heating elements along its length, a pulling unit and a flying cut-off saw. Temperature profiles along the die, pulling force, pulling speed and pressure inside die are measured and recorded in data form. Hydraulic oil pressure exerted during pulling is monitored through PLC-controlled pulling unit. This pultrusion pulling unit can either be used for open bath or closed die pultrusion. In our regime, open bath pultrusion with 300-mm discontinued tapping section was used as shown on Fig. 1b.

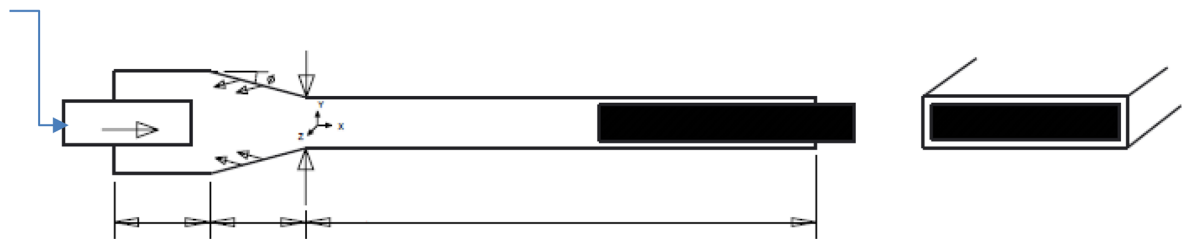
Wetting of reinforcing fibres is very crucial for any composite part without dry patches. In open bath (Fig. 1b), impregnation technique used to wet fibres is achieved by pulling fibres through the resin tank. In order to ensure all fibres are sunk under resin, resin label is not allowed to go down below specified limit. Higher pulling speed and entangled fibres are avoided for better wettability. Impregnated fibres are guided through guide rollers and plate and finally through preforming assemble to have specified part cross section prior to entire into die. When pulled through the resin bath, excess of resin carried by roving at die entry will

Table 2 Formulation and conversion in dead-end polymerization experiments

Initiator MEKP	0.25	0.32	0.40	0.48
Residual heat (J/g)	239	230	212	176
Conversion (%)	27	30	42	50



(a)



(b)

Fig. 1 **a** The schematic of the open bath pultrusion line. **b** The schematic of compaction zone in conventional pultrusion die

wet-out cloths like polyester veil or glass veil. Discontinued compaction taper section assists in squeezing out excess resin and trapped air to get void free pultruded parts (typically between 1 and 5% vol.). Curing to solidification of profile is made by passing the squeezed material through heated die. Die temperature management is crucial in order to produce good quality components; hence, a gradual increase in resin temperature is achieved by placing more heating zones with different set temperatures along the length of the die time of mat entry during travelling through die and was recorded by the thermal sensors placed between the fibre pack. The fibre-package consisted of 10 layers of Bidirectional mats with 600 g/m^2 and 60 roving with 4800 tex. The thickness of the produced composites was 8 mm of high-pressure taper die (Fig. 1b).

Many variations on trials were conducted on adding additional mats, on the high-pressure conventional dies. Add-on reinforcing method in pultrusion is used to find pull

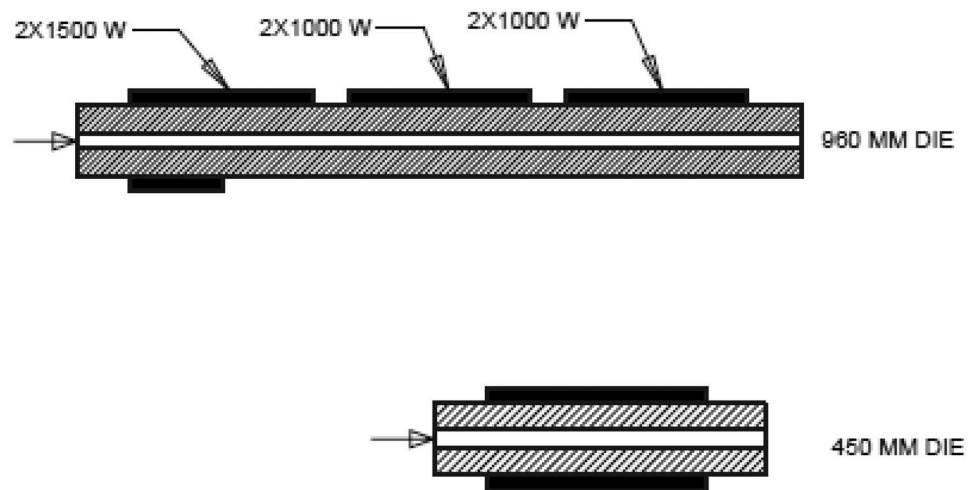
force throughout the die used at different speed and filler loading; the temperature at surface and core during pulling is also recorded. To trace the magnitude of pull force change, additional mats, 200 mm wide and 254 mm long, were inserted in the centre prevailing fibre pack. The speed of pulling was set at 20–50 mm/min. Thermocouples were placed in between the mats to measure the temperatures of core and surface as well. The pulling speed was set at different speeds like 20 mm/min and 45 mm/min. As the mats travelled through the die, the time mat entered the die was recorded and based on speed; axial distance is calculated against pressure appeared. The experimental result for the high-pressure conventional die with extra tapping section is shown in Fig. 1b. It is planned such that pulling force magnitude positions front edge of the additional mats traveling along the die and y-axis, pulling force magnitude positions die-centre towards wall pulling is recorded separately for each driving forces which governs the ultimate pull forces.

The ‘add-on reinforcement’ in the pultrusion operation was conducted using the conventional die with discontinued specially designed 0.3-m taper section as shown in Fig. 1b. As compaction zone is predominating on other frictional forces, separate experiment for downstream part of the die which undergoes resin drag and dynamic friction before gelling is required to conduct at room temperature. A short-length and long-length dies without taper portion were used to comprehend contribution of friction of viscous zone and influence of its subsequent length. Furthermore, influence of die length on pulling force was investigated using different die lengths. A

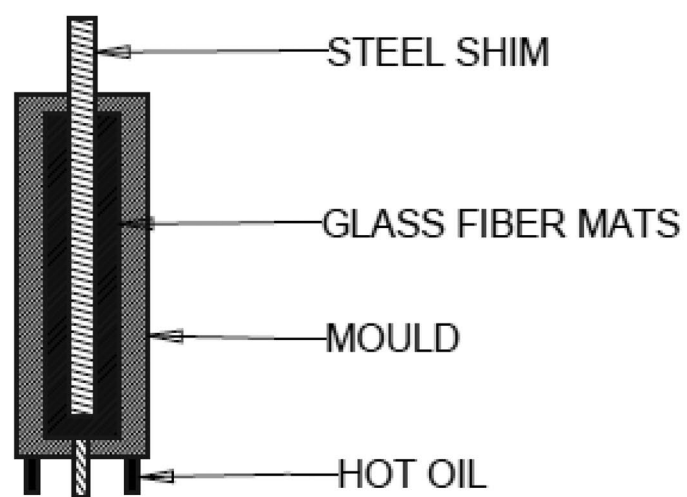
1200-mm, 800-mm and 500-mm three conventional dies were employed in this experiment. The pulling speed and the fibre package remained unchanged as used in add-on reinforcing method. Schematic of the experiments in short die and long die is shown in Fig. 2a, b. All along ‘low fibre volume fraction’ were maintained in short and long dies.

Pull force arises from friction between composite and the die surface predicts the effect of temperature, resin conversion, pulling speed at gelling and post gelling region, anticipating shrinkage and thermal expansion of the product.

Fig. 2 **a** The schematic of short straight die length, **b** the schematic of side view of the mould used to predict the pull force in liquid zone



(a)



(b)

As shrinkage coefficient is governed by conversion of polymers and the filler loading in resin. Composites with different shrinkage factors were considered in conducting trials. The short 500-mm single cavity die as mould was used to find the compressive stress during compaction at different thickness and steel shim placed beforehand in the die was pulled to record pulling force against time for straight portion at different temperature, resin conversion and pulling speed. Compressive stress and pulling force required was recorded by an Instron universal testing machine (Model-Delta-C200-10 Tons). The side-view of the mould is also shown in Fig. 2a, b. Experiments were conducted on the same short die but keeping length of the steel plate long. Arrangement is made in such a way that the plate is three times longer than the mould to keep the contact area constant throughout the experiment. The experiment was conducted for three different filler loading in a resin of specific shrinkage factor, for two resins of different shrinkage factor at 105 °C constant temperature. In the experiment, the plate was wrapped with resin impregnated glass fibres at different % conversion.

The resin was formulated to have different % conversion and steel plate was pulled for a span of 6 min at speed of 10 mm/min. Formulated resin as listed in Table 1 is used in impregnating reinforcing materials and two layers of random mats with surface veils used for wrapping steel plate. Percentage conversion is controlled by placing reinforcing materials in a preheated 90 °C mould with specific thickness and maintained heating for 30 min. The heated plates for that period are long enough to run out the initiators from Parkadox-based formulated resin system. Different % conversion was confirmed by the DSC before keeping on the single cavity mould holding amid the steel shim. The mould was completely closed and pulling test was performed in three different stages. In the first stage, steel plate was pulled out by one-third of the total length at room temperature followed by 60 °C and 105 °C for remaining subsequent shim length. All along, 200 mm/min pulling speed was maintained and pulling force exerted due to friction recorded. Several impregnated partially cured fibre mats were first wrapped by surface veils as used in actual pultrusion process, then laid up evenly in both mould halves. A chromed steel shim of 2.0 mm in thickness and 90 mm in width and 300-mm length was placed between the fibre reinforcement materials, and the mould was then closed. The dimension of the mould cavity was 8 mm thick, 100 mm long and 100 mm wide – the initial contact length of the plate and the fibre mats was 100 mm, thus the initial contact area of 90 mm by 100 mm. To prevent fibres from moving up during pulling high-fibre volume, fraction was maintained thereby providing a high holding force.

Steel plate out of the mould at a constant speed was pulled gradually and force change versus time was recorded by

Instron universal testing machine tester. From known cross-sectional area, pressure can be calculated wherein friction of coefficient obtained is pulling force divided by the contact area and the compaction stress. In investigating temperature effect on friction, heating tape was used on steel shim, wherein change in temperature was monitored. Liquid region friction experiments at different temperature were carried out by wrapping prepreg with different % conversion on steel plate placed into the mould as described in pultrusion operation. Similarly, material described in pultrusion method, resin with different filler contents like 10, 30 and 40 phr, was used.

3 Results and discussion

3.1 Pull force modelling

The pressure accounts force due to compaction at tapping zone, friction due to viscous drag and friction due to cured product with die surface. The modelling and simulation are strongly dependent on many physical process variables which need to be investigated. Many models are available in the literature such as the thermo-chemical modelling, fluid dynamics modelling, and thermo-mechanical modelling employed to investigate behaviour change in pressure experienced by the fibre pack during pulling through die. Three pressures that fibre pack being experienced mainly during drag are compaction resistance, viscous resistance and friction resistance (dry fibres and solid profiles with die surfaces).

Compaction resistance is mainly due to resistance of fibre bed to get squeezed during compaction depending on fibre volume fraction influenced by porosity of fibres and permeability of resin [23–30].

$$\delta = F * L^3 / (192E * I) \quad (9)$$

$$L = \beta * (l_0 - l_{min}) \quad (10)$$

$$\delta = (l_0 - l) \quad (11)$$

$$\text{Assuming } l_{min} = d,$$

$$P = F/L * w = [(l_0 - l)192 * E * I] / \beta * (l_0 - d)^3 \dot{w} \quad (12)$$

$$B \text{ is bending stiffness} = 192 * E * I \quad (13)$$

$$\text{considering, } \dot{w} = L,$$

$$V_f = \pi d^2 / 4 l^2 \quad (14)$$

$$V_0 = \pi d^2 / 4 l_0^2 \quad (15)$$

$$V_a = \pi/4 \quad (16)$$

where ‘ L ’ is length of the fibre segment, ‘ E ’ is modulus of the fibres, ‘ d ’ is diameter of the fibre, ‘ I ’ is inertia of bending of the fibres, ‘ F ’ is contact force of the fibres, ‘ l_0 ’ is initial height of the prism, ‘ l_{min} ’ is minimal height, ‘ l ’ is height, ‘ β ’ is constant by microscope span height to span length ration of fibres network, B is bending stiffness.

$$P = 3\pi B[\sqrt{(V_f(x)/V_0)} - 1]/\beta^4[\sqrt{(V_a/V_f(x))} - 1]^4 \quad (17)$$

This was modified by Carlone et al. formulation [25] for compaction zone with index $\hat{n} = 2$. By principle of porosity in conical die,

$$\{V_f(x)\} = (h_L * V_f)/[h_L + (L_m - x) * \tan\theta] \\ P = (3\pi B/\sqrt{\epsilon})[\sqrt{(V_f/V_0)} - \sqrt{\epsilon}]/\beta^4[\sqrt{(V_a * \epsilon/V_f)} - 1]^2 \quad (18)$$

where

$$\epsilon = 1 + 2(L_m - x)/h_L \tan\theta \quad (19)$$

Fibre volume fraction can be calculated by deciding N_r (no of roving in any particular volume). Where N_r is the number of roving used in the specific volume and L_w is the linear weight of fibre. Final volume fraction of um-reinforcing material [11, 14, 22] is a quantitative value of porosity (Φ), i.e. $(1 - V_f) = \Phi$, and permeability (K) as proposed by Henry Darcy is

$$V_f = N_r * L_w / (A * \rho_f) \quad (20)$$

Theoretical values used in model fitting of $V_0 = 0.350$, $V_a = 0.785$ square and 0.907 for hexagonal, $\beta = 2.54 * I = 2.61 * 10(-7)$, $E = 8.2 * 1010$, $\rho_f = 2620 \text{ kg/m}^2$, $L_w = 4800[\text{tex}]$ for glass,

$$\int dP_f = \int (3\pi B/\sqrt{\epsilon})[\sqrt{(V_f/V_0)} - \sqrt{\epsilon}]/\beta^4[\sqrt{(V_a * \epsilon/V_f)} - 1]^2 dx \quad (21)$$

This is the pressure experienced by fibre beds not by the resin or matrix. Hence, compaction pressure on matrix is evaluated.

$$U_x = (K/\eta) * \delta P \quad (22)$$

where U_x is the resin flow speed, K is the permeability and η is the resin viscosity, and δP is the pressure gradient and Permeability by Carlone et al. [27]:

$$K = d^2(1 - V_f)^3 / Kc * V_f^2 \quad (23)$$

From fibre continuity,

$$V_f(x) * h(x) = V_f * h_L \quad (24)$$

Since,

$$[h_L/h(x)] = (V_f/V_0) + (1 - V_f/V_0)x/L_m \quad (25)$$

$$V_f(x) = V_f / [(V_f/V_0) + (1 - V_f/V_0)x/L_m] \quad (26)$$

From matrix continuity [28, 29] on volumetric flux,

$$Q(x).h(x) = U_x(1 - V_f) * h_L, Q(x) = U_x[(V_f(x)/V_f) - V_f(x)] \quad (27)$$

Relative matrix flux

$$Q_R(x) = [Q(x) - U_x(1 - V_f(x))] = U_x[(V_f(x)/V_f) - 1] \quad (28)$$

Since apparent viscosity of the Carreau model may be written as follows:

$$\eta_a = \eta_0(1 + (\lambda * \gamma)^2)^{(n-1)/2} \quad (29)$$

From Darcy equation, $P = (U_x * \eta)/K$,

$$(dP/dx) = [Q_R(x) * \eta]/K \quad (30)$$

$$(dP/dx) = Q_R(x) * \eta_0(1 + (\lambda * \gamma)^2)^{(n-1)/2} / K \quad (31)$$

γ = shear rate or velocity divided by layer distance,

$$dP/dx = \frac{[Q_R(x) * Kc * V_f(x)^2 * \eta_0[1 + (\lambda * \gamma)^2]^{(n-1)/2}]}{d^2(1 - V_f(x))^3} \quad (32)$$

By principle of porosity in conical die,

$$\{V_f(x)\} = (h_L * V_f)/[h_L + (L_m - x)\tan\theta] \quad (33)$$

Now as per pressure gradient by Dong law [5, 8, 27],

$$\frac{dP}{dx} = \int \frac{dP_d}{dx} = \int \frac{G \cdot \eta \cdot U \cdot V_f^2 \cdot h_L^2 \cdot (L_m - x) \tan\theta}{d^2 * [(1 - V_f)h_L + 2(L_m - x)\tan\theta]^3} dx \quad (34)$$

where Gebart, defined shape factor G , as 57 for a quadratic fibre arrangement [31, 32]. Since P_d is pressure due to drag, it would be considered only because of matrix and for fibres bed reacting is the P_f . Hence, compaction pressure is a combined effect of matrix and the fibre bearing load. Compaction resistance is predominantly influenced by taping angle, fibre volume fraction speed of pulling and part thickness. In predicting resistance, initial taping angles θ radian is potentially considered for models but principally taping angle varies with axial distance which needs to be considered for fibre beds. Fibres close to core are experiencing less bending compared to fibres close to surface. Hence, in this study, ‘ θ_f ’ an average angle was calculated considering the gradient of change in taping angle depends on length of compaction zone and shape factor of reinforcement.

$$R = \int (\theta - 1.47 * Z.^3), 0.000 < Z < 0.25), \theta_f = (R./0.25) \quad (35)$$

$$\int dP_c = \int P_f \cos \theta_f * \sin \theta_f dx + \int P_d \sin \theta_f dx \quad (36)$$

Viscous resistance is believed to be drag resistance influenced by viscosity of resin and drag speed. Viscosity is a direct implication of the shear stress on composite surface before complete curing between gelling and post gelling phase [30–35].

$$\int dP_v = \int (\eta_a U / r \cos \hat{\theta} dx \quad (37)$$

$$\int dP_v = \int ((\eta_0(1 + (\lambda * \gamma)^2)^{(n-1)/2}) U / r * \cos \hat{\theta} dx \quad (38)$$

r is the distance between the layers or fibres, varies with fibre arrangement [8, 31, 35] like

$$r = d(1 - \sqrt{((\sqrt{3})(\pi V_f(x))/2)/2}) \quad (39)$$

But in our study, adhesion of resin layer to the surface of die plays additional roles and is influenced by increase speed lessens heat effect on viscosity of resin (stress \times gradient of speed). $\cos \hat{\theta}$ was called liquid–solid affinity, where $\hat{\theta}$ was contact angle of liquid–solid phase and σL was interfacial surface tension of solid-slurry. Infiltration and permeation ability of the liquid resin is directly influenced by affinity of the liquid and higher adhesion force. The monitored die surface decreases affinity between liquid resin and solid die surface. Since the viscosity changes with time influenced by heat, the average viscosity was considered in our study.

Considering the initial practical viscosity of the resin used as 0.4 Pa.s, the average viscosity can be calculated as follows,

$$\int d\eta_v = \int (0.4 * \exp(.0894 * t) dt, \quad (40)$$

$$0 < t < (x - L)/U$$

while the adhesion load is,

$$\int dA_d = (520 - (0.025 * (\eta_v / (x - L_m) / U)) * 2 * 3.14 * h \quad (41)$$

$$\begin{aligned} \int dP_v &= \int (\eta_0(1 + (\lambda * U/r)^2)(n-1)/2U/r) * \cos \hat{\theta} dx \\ &+ \int (520 - (0.025 * \eta_v / (x - L_m) / U)) * 2 * 3.14 * h_L dx \end{aligned} \quad (42)$$

Friction resistance arises from dry fibres and solid profile with die surface is presented as,

$$\int dP_f = \int P d(x) * f * \cos^2 \theta(x) dx \quad (43)$$

where f is the friction coefficient. When the surface of the composite is solid, the expression is considered as normal stress between composite and die.

In our study, pull force model for friction resistance, shrinkage-induced part detached pressure which plays additional role to reduce friction is considered. Hence, the existing normal stress between die and solid profile gets reduced by $(\hat{G} \delta R / r)$ helping to get part detached. Theoretical bulk modulus of the resin is $\hat{G} = 4. * 10^8$, and $0.75 < x, 1.5$, [4, 5, 28] wherein G -Bulk Modulus, δR -shrinkage of resin and $\hat{\lambda}$ -resin layer thickness. δR is the shrinkage of part which can be assumed as change in length since the radius parameters such as the shrinkage factor (S) of the resin, layer thickness ($\hat{\lambda}$) and extent of curing controls normal stress as modified to are as follows:

$$\int dP = \int (\hat{G} * (r) / (0.2 * (x)) dx \quad (44)$$

$$\int dP_{ef} = 0.085 * \int dP_f - \int dP \quad (45)$$

3.2 Start-up experiments and slip phenomenon

As shown on Fig. 3, during start-up stage, two different situations are analysed. One where reinforcing fibre saturated with only pristine resin and another wherein resin contains 30-phr filler and 5.5-phr nanofillers are pulled through the conventional ‘open bath’ discontinued taper die, maintaining 50 mm/min pulling speed. The pulling force trajectory

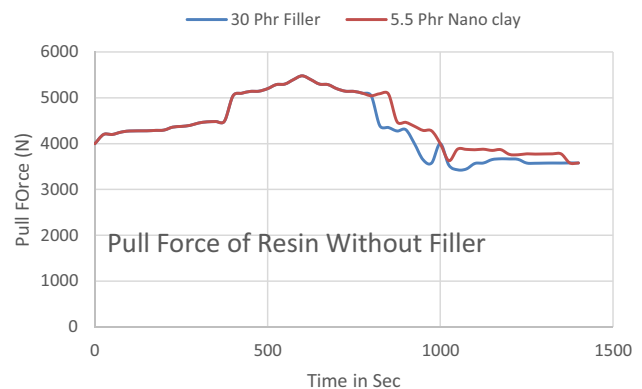


Fig. 3 Effect of with and without filler during start up pulling

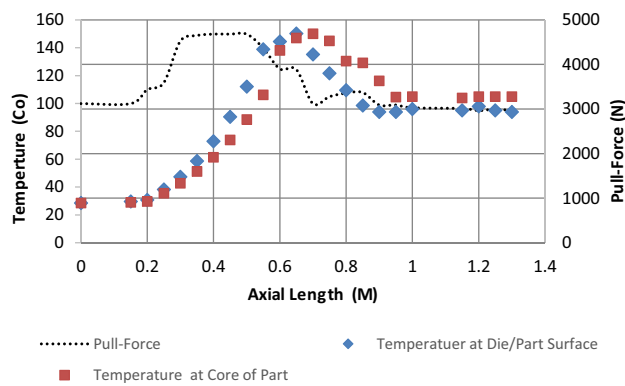


Fig. 4 Measured values for changes in temperature at core and surface and pull force during pulling along axial length

against times of Fig. 3 shows that dry fibre package pulling pressure reaches to maximum at 625 s and leads to 5398 N force but after about 650 s as pure resin began to run out, pressure drops and leads to 3429 N force for a specific area die profile. The shoulder of decrement observed faster for 30-phr filler loading in respect to 5-phr MMT-treated nano filler. This experiment indicates that friction is more for wet fibres with nano fillers but more vulnerable for dry fibres. The probable explanation could be due to interface layer thickness of resin which minimises the friction between fibres and die wall. The thicker the layer of resin as in case of higher viscosity due to higher filler content and less, as expected for pure resin and low-dosed nano fillers, the less would be the friction in between reinforcing fibres and die wall. Fillers are an essential component in the resin formulation which must be configured to have corrosion and heat resistance with good surface finish at low cost.

3.3 Compaction effect by add-on reinforcement

Unlike the analytical and simulation model [36] in the literature, our study shows sudden rise in pressure rise from 0-bar to 160-bar and then gets to plateau initially as the add-on reinforcement travels through die as shown in Fig. 4. In fact, the pull force trajectory remained unchanged until 100 mm but follows sinusoidal pattern to reach maximum value (4680 N) and gets stabilised subsequent of gradual decrease in pressure. This sinusoidal trend of increasing of peak and resuming original value is noticed as fibre pack travel moves down axial distance. Indeed, peak gets broaden followed by gradual increase at initial compaction and drops insidiously until tapping angle gets flattened but hardly any change is observed in overall pulling force, for additional reinforcement.

Temperature change near the surface and inside the composite is recorded by thermocouples placed in the fibre package, one at just beneath the surface veil and another in the middle of fibre package. It is observed that rise in temperature is barely perceptible until the compaction zone ends, but interestingly, temperature change caused by the exothermic resin reaction just before 300 mm away of exist end reached its maximum value. This implies that the rest of the pulling force develops in late stream zone and is due to the gelling effect and solid friction post-curing. This implies composite cohesive force gets debilitated to die surface facilitating loose contact before the reaction peak temperature.

In the literature, the simulation model [36] shows the rise in pressure observed after traveling certain axial distance (300-mm) of die inlet. In contrary, our study observed (Fig. 5), decreasing compaction tapping angle right from die entry while the magnitude of pull force increases and vice versa. The peak

Fig. 5 Measured values for changes in pull force during pulling at varying degree of compaction during pulling operation

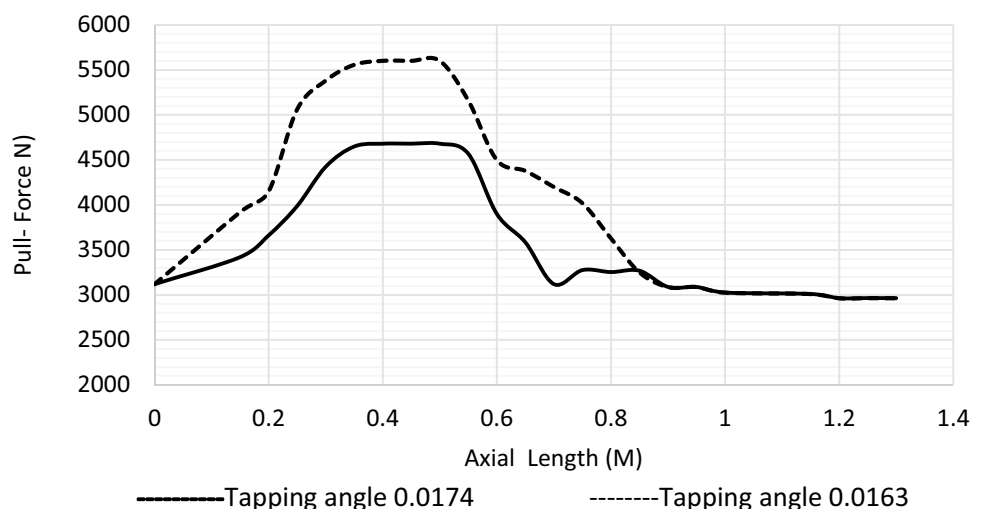
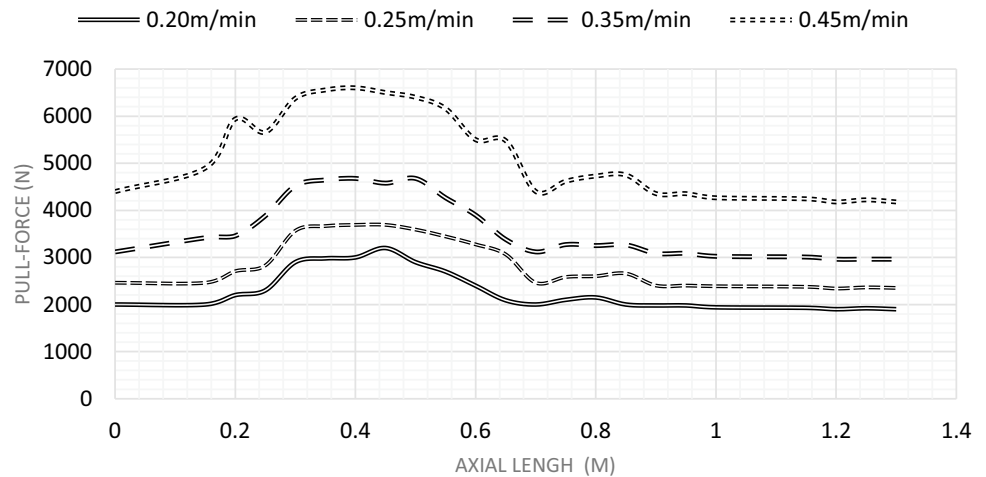


Fig. 6 Measured values for changes in pull force at different experimental pulling speed along axial distance



was observed at the entrance flat portion of die which experiences major compaction. Again, the late stream part of the die has less response to the additional mats, but a flitting response pattern was observed with decreasing tapping slope.

Figure 6 shows the similar trend in increases of pulling force with increasing pulling speed from 0.2 to 0.45 m/min. Response to pull force is higher and sensitive to higher speed similar to studies found in Ref. [36] wherein pressure

Fig. 7 (a) Stable product in operation during pultrusion pulling. (b) and (c) Scaling of product in operation during pultrusion pulling. (d) Part failure in operation during pultrusion pulling



(a)



(b)



(c)



(d)

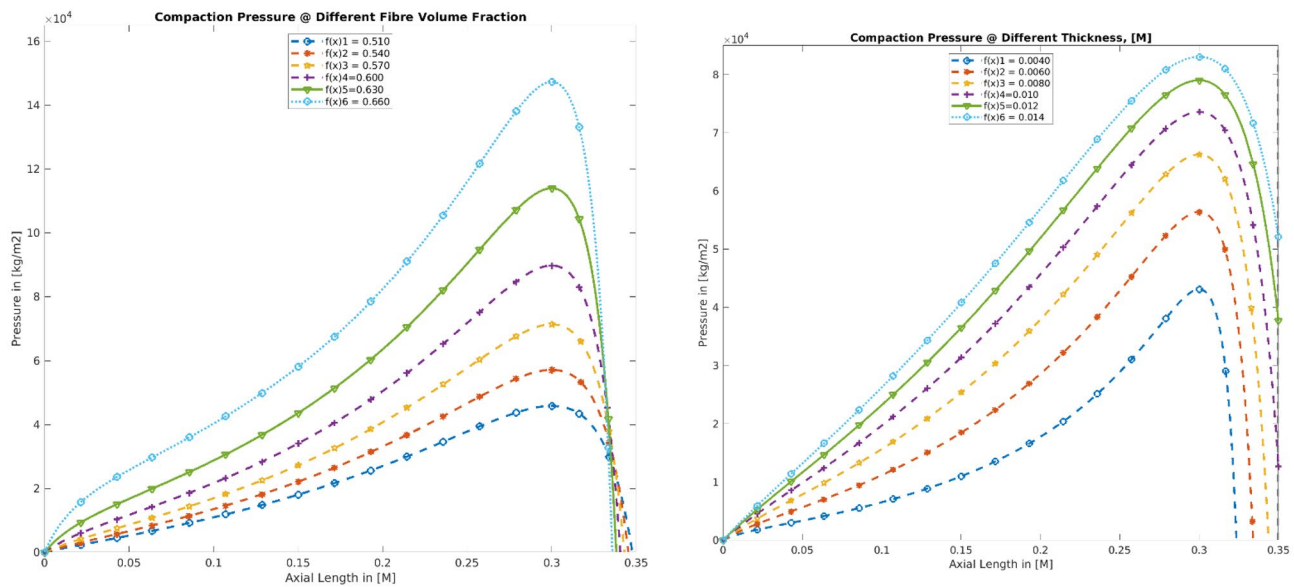


Fig. 8 Experimental results showing the influence of (a) fibre volume fraction and (b) profile thickness on compaction pressure during pulling

increased from 0–80 and 0–68 bars for higher and lower speed with similar tapping angle. A possible explanation is that initial pull force is the existing pull forces and for any additional reinforcement at compaction experiences more pressure to accommodate the solid reinforcement into final die gap squishing out excess viscous resin. Viscous drag forces (mainly late stream) part of the die to contribute marginally unlike compaction forces of total pulling force [6, 8, 33, 37].

Hence, of a good understanding parameters in scale-up operation to get stable product (Fig. 7a) are crucial otherwise, one may encounter problems like over curing of the parts and eventually loss of heat, warpages of the product due to uneven curing, low productivity due to slow pulling speeds, scaling at part edge (Fig. 7b, c), seizure of dies and ultimately line/part failure (Fig. 7d), higher pulling force required leading to higher electrical (energy) consumption during manufacturing stage.

In our study, MATLAB software was employed and influencing parameters including fibre volume factor, tapping angle of die, thickness of the profile and drag velocity were computed in model fitting and correlated to the experiments results. It was found that proposed model results were in good agreement with degree of compaction as recorded experimentally. It is worthy to mention that we are restricting axial length separately for compaction from 0 to 0.3 m and where in 0.3 to 1.5 m experienced flat portion for pressure due to viscous and friction. From model fitted 2D graphs (Fig. 8), paradigm of compaction pressure changes with sweeping fibre volume fraction, drag speed and profile thickness as appeared

which are similar to recorded experimental results but rising trajectory is sharp, prominent and clear. In model fitting, variables like tapping angle ranges from 0.014 to 0.019° radian, fibre/volume fraction varied from 0.480 to 0.620, part thickness ranges from 0.004 to 0.014 Mt and drag speed varied from 0.0020 to 0.0032 m/s.

Using the governing Eq. (36) as derived from Eqs. (9)–(35), compaction pressure is plotted against many complex variables. It is found that tapping angle has negative influence on pressure which shows sensitive to higher values of variables when plotted in 2D graphs as shown in Fig. 8a, b. Pull force appeared sharp increase and lasts longer for thick profile but drops insidiously unlike thin profile, wherein sudden drops in pressure observed of parameters like fibre volume fraction and speed of pulling. With increasing speed and tapping angle, change in pulling pressure is plotted. Similarly, as shown in Fig. 9a, b, increased pull force is perceptible profoundly for increasing velocity, but difference is barely perceptible for dropping pressure, wherein for increased tapping angle shows long lasting pressure along axial distance (Table 3).

3D-surface plotting as shown in Fig. 10a depicts nature of pressure drops swiping thickness as functional parameters long axial distance. Spikes appeared prominently sharp and profound for 'higher speed' and 'tapping angle' deviating shifting harmony in axial distance. Similarly, Fig. 10b depicts paradigm of increased pressure swapping speed of pulling or drag velocity as function maintaining shifting harmony in axial distance. A comparison between measure values with model fitting is elicited in Table 2.

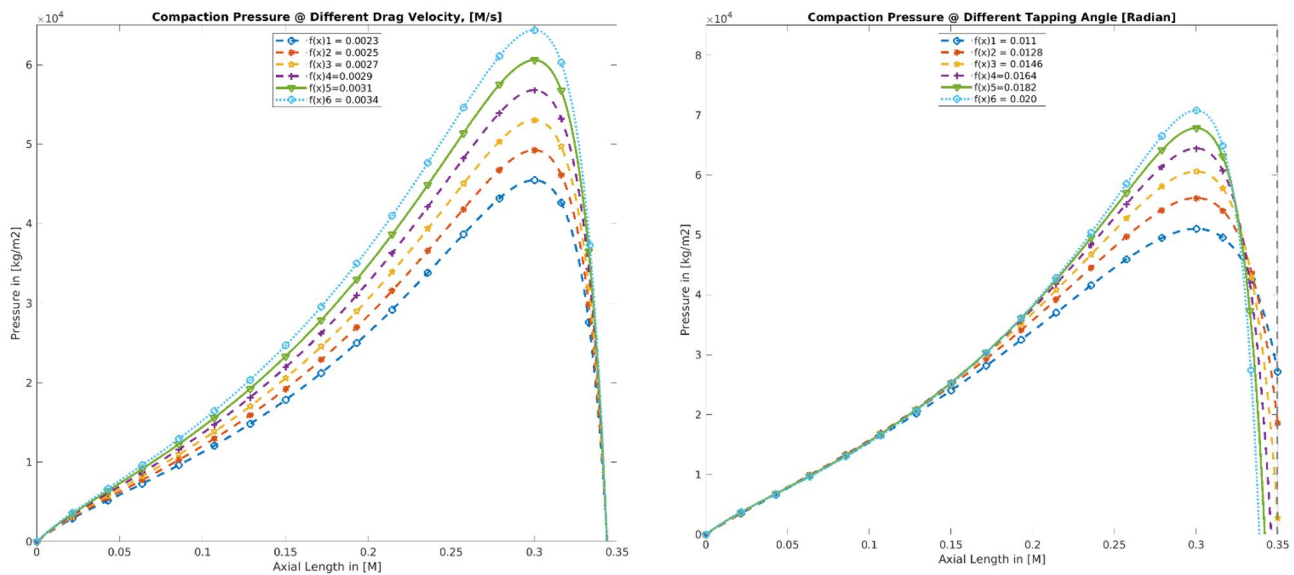


Fig. 9 Experimental results on the influence of (a) pulling speed and (b) tapping angle on compaction pressure during pulling

3.4 Viscous force phenomena in liquid phase

To investigate the viscous force phenomena in liquid phase, experiment were conducted to investigate the contribution of viscous drag force to total pulling force. As shown in Fig. 11, pulling force at 80 mm/min speed, both dies (450 mm and 960 mm) show no significant change at liquid phase. Hence, increased length of straight portion in die makes no difference with shorten die length unless viscosity gets influenced by temperature, pulling speed and fibre volume fraction. Before gelling as indicated in the add-on reinforcement method, the pultrusion die does not minor contribution to the pulling force; similarly predominantly in liquid phase, straight portion of longer die length cause no increase is pulling force. Pulling force in this region was only due to reaction and stimulated gelling and post gelling resin until the surface solidification.

3.5 Viscous force verified by steel-shim

A thin liquid layer that exists between fibres and the die surface in the liquid zone has been assumed in the literature [38, 39] and it is the controlling factor of pull force and increases with increasing pulling speed or assumed proportional

to overall pulling force. The phenomena are witnessed by compaction and viscous zone irrespective on influence of temperature.

The concoction behaviour of the resin gelling from liquid and subsequently to solid during operation through pultrusion die is very deceptive to comprehend. Viscosity gets burgeoned rapidly on gelling of resin, due to viscous friction at die surface. At die-composite interface, such mechanism of viscous friction could be influenced by resin conversion and temperature. Hence, it is intrigued to investigate the influences of processing parameters on friction force. A short-length die with steel plate was used to comprehend influence of temperature, conversion, filler loading of resin on friction of viscous zone. In experiments, heating tape wrapped around steel plate placed inside short die equipped with temperature controller, to facilitate to have different temperatures as described above. Process of controlling % conversion of resin and testifying the same by DSC was discussed above. In friction measurement process, different final conversion is achieved by adjusting reaction temperature, reaction time and amount of low temperature initiator (MEKP) [18–21, 42, 43]. Perkadox-C is also a low temperature promoter which synergise the influence of MEKP at a particular temperature. Benzol peroxide (BPO) an initiator is mixed with promoter tertiary butyl per-benzoate (TBBP) to have conversion at higher temperature.

Table 3 Comparison between model fitting and measured values

Effects on	Tapping angle (Radian)		Speed of pulling (m/min)			
	0.01734	0.0163	0.2	0.25	0.35	0.45
Pull-force measured (max in N)	5600	4568	3200	3690	4680	6600
Model fitting-pulling pressure (max in kg/m ²)	6.95×10^4	6.4×10^4	5.89×10^4	6.43×10^4	—	—

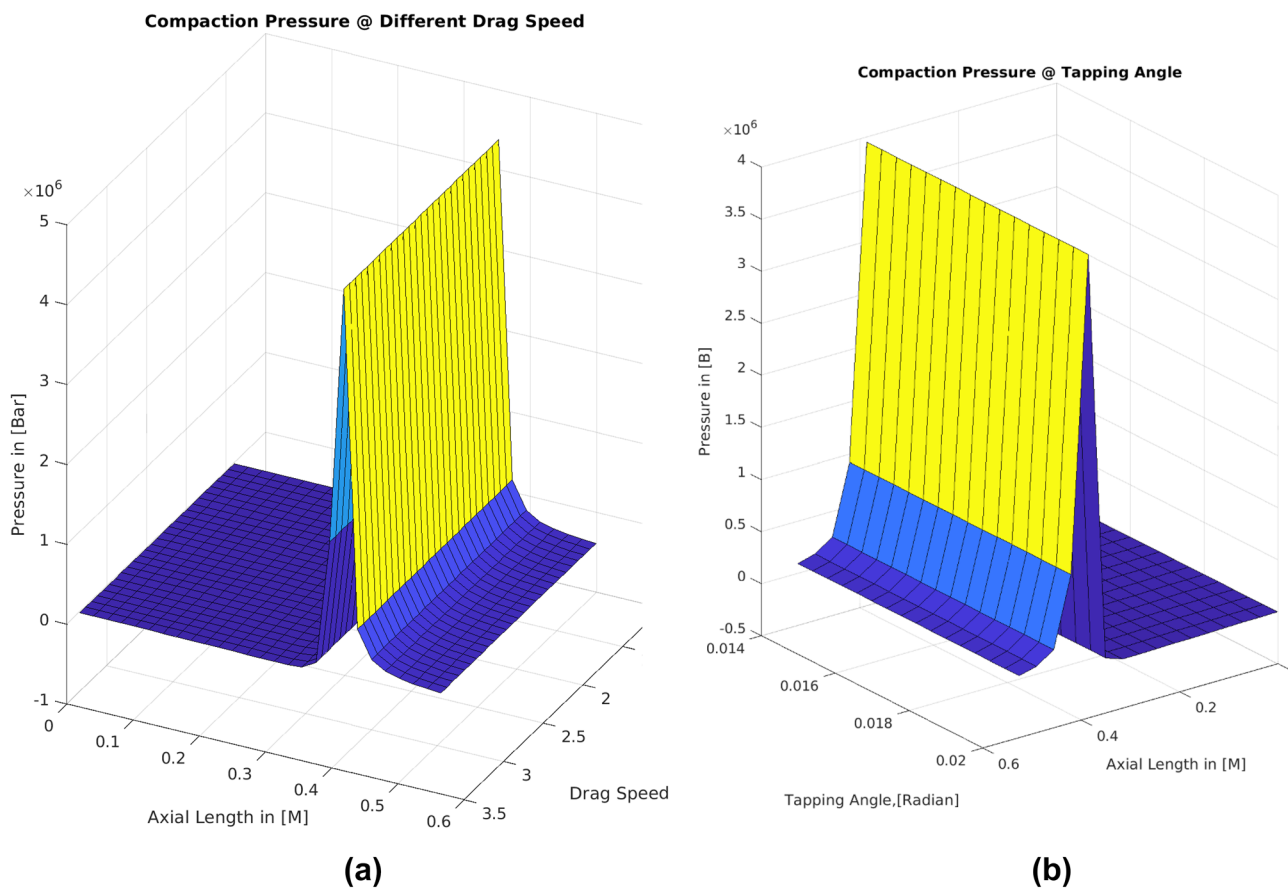
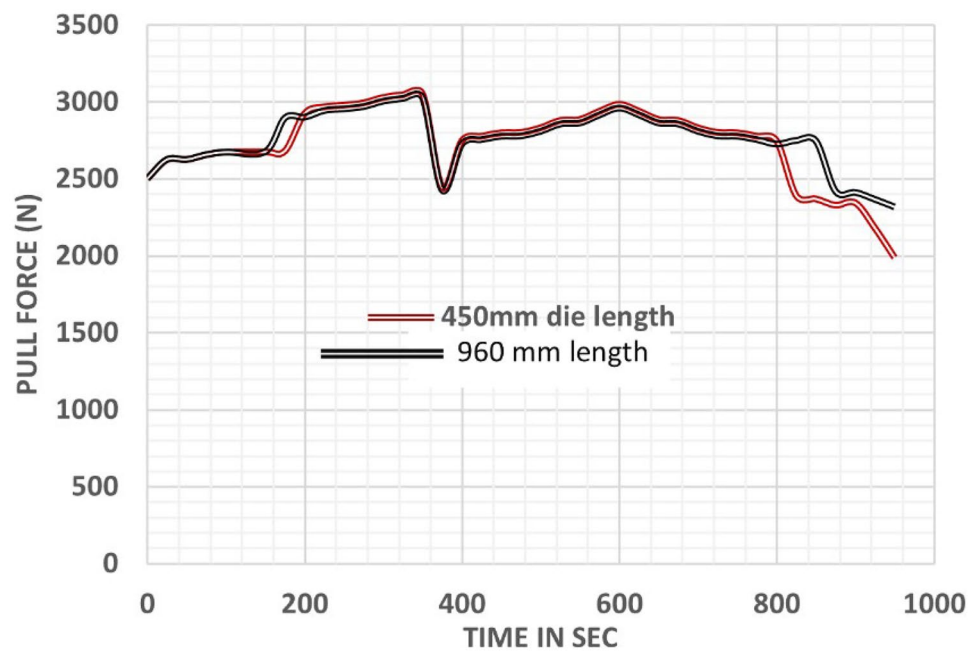


Fig. 10 (a) 3D surface plot on influence of tapping angle on compaction pressure and (b) 3D surface plot on influence of profile thickness on compaction pressure

The friction is the direct implication of pull force and can be measured as function of both parameters' temperature and

resin conversion. The stress normal to die surface is recorded by the pressure transducer. Pulling force required to pull thin

Fig. 11 Effect of speed and die length during pulling in liquid zone before solidification



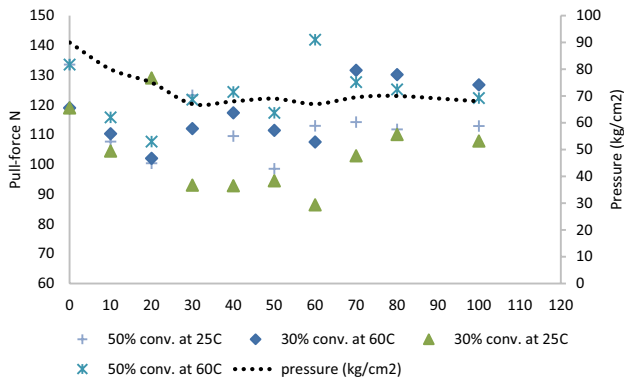
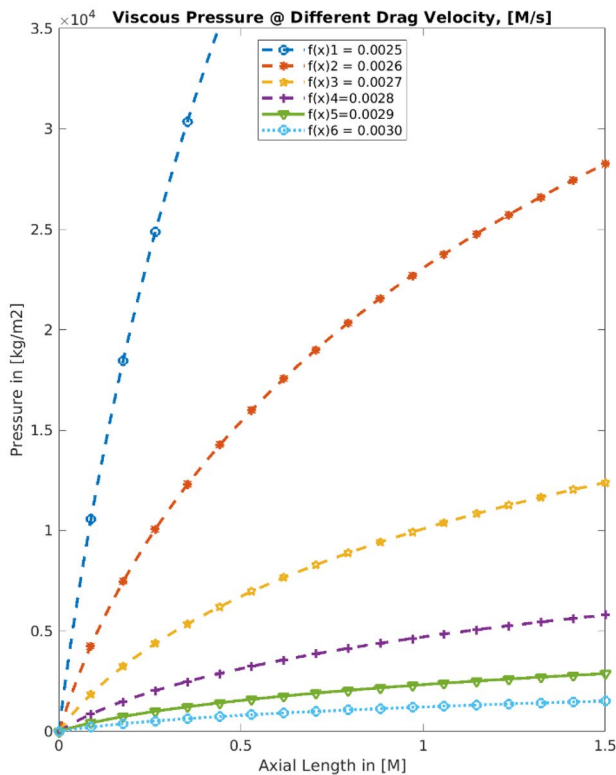


Fig. 12 Pull-force recorded using device for viscous drag during pulling

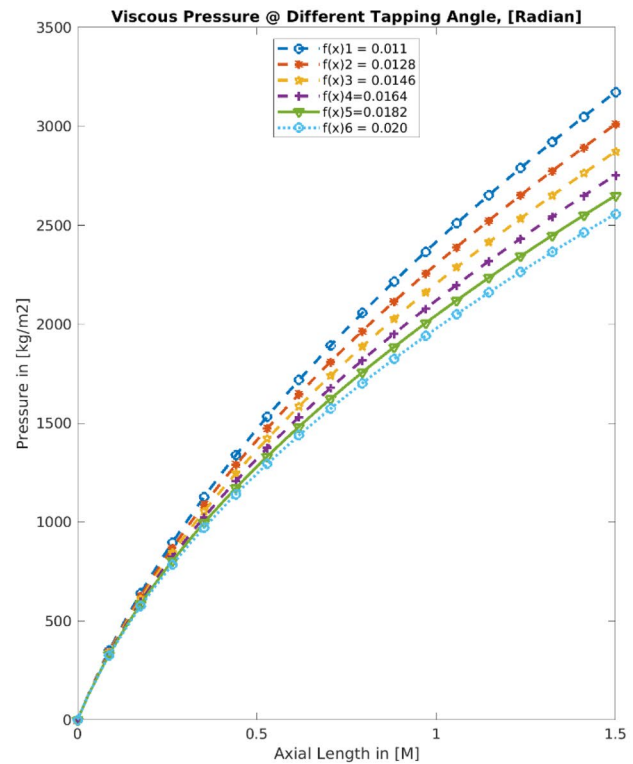
plate is comparatively low but it is reasonable to compare pressure. There are initial drops in pressure due to drops in viscosity, but tension starts rising with passing secs. The most probable explanation would be due to shear thinning due to heat and shear effect of unreacted polymers and monomers facilitating pull force to decreased greatly [34, 35, 37], which may further be influenced by increasing speed. Further in the event of different % conversion at different temperatures, nature in changing

friction and stress inside during viscous drag at gel and post-gelling region is shown in Fig. 12. Pull force for 30% conversion recorded at room temperature (25 °C) is higher compared that at 60 °C, wherein the difference is more profound at 50% conversion resin-impregnated fibres. This indicates that friction due to viscous drag becomes larger when resin is at ‘gel state’ and with increasing temperature at any given constant contact pressure situation gets more vulnerable for higher molecular weight resin. As the matrix starts crosslinking, affinity to die surface lessen and eventually reduced adhesion force is presumed but rising viscosity increase pulling force in viscous phase. Overall trend implies that higher temperature are more influential than the lower temperature regime in that it promotes crosslinking hence maximising the resin viscous condition.

Similarly, using governing Eq. (42) as derived from Eqs. (37)–(41) and subsequent model fitting by using MATLAB software considering simulations were computed to compare experiments results. The study accounted for a series of parameters including drag velocity, fibre volume fraction, thickness of the profile and tapping angle. In our study, adhesion force is considered which contributes significantly at low surface tension between solid and liquid surface interface. The surface tension directly varies with viscosity and that varies with speed. As drag speed increases,



(a)



(b)

Fig. 13 Influence of **a** fibre volume fraction and **b** profile thickness on viscous pressure during pulling

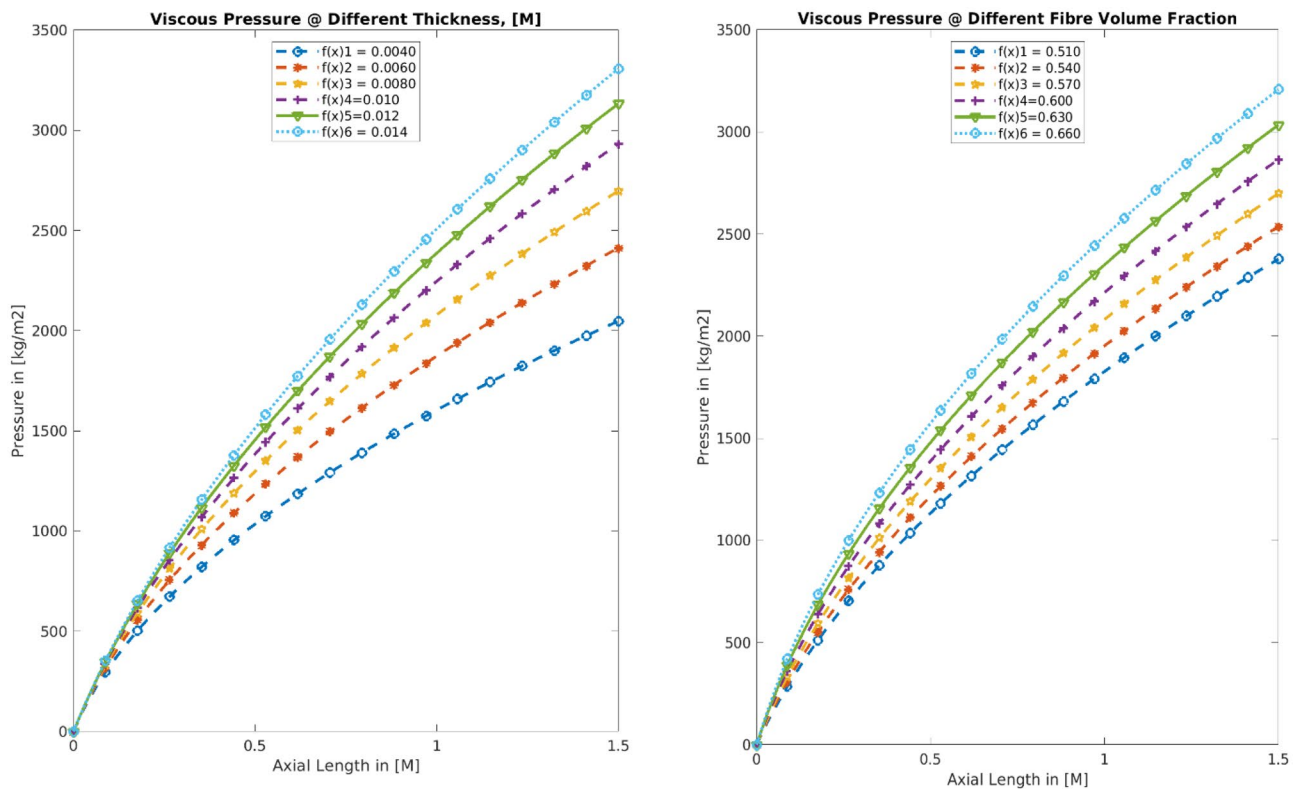


Fig. 14 Influence of (a) fibre volume fraction and (b) profile thickness on viscous pressure during pulling

contribution of adhesion force to total viscous force is less significant. Hence, average viscosity was taken during fibre pack travel in the flat Sect. 2D-plot as shown in Fig. 13a, it was found out that viscous pressure responds promptly with increased drag velocity; wherein in Fig. 13b, similar behaviour as observed in compaction pressure, pressure shows decremental with increasing tapping angle. Figure 14a, b for

change in profile thickness and fibre volume fraction shows similar paradigm as observed in compaction, but the overall contribution to total force is less. It is worthy to mention that axial length is restricted to 1.5 m for flat portion. From the model, it is evident that paradigm is incremental and reaches plateau due to increase in viscosity which in turn leads to gelling and subsequently to solidification. Gelation process

Fig. 15 Pressure/pull-force recorded of polyester resin at different characteristic shrinkage

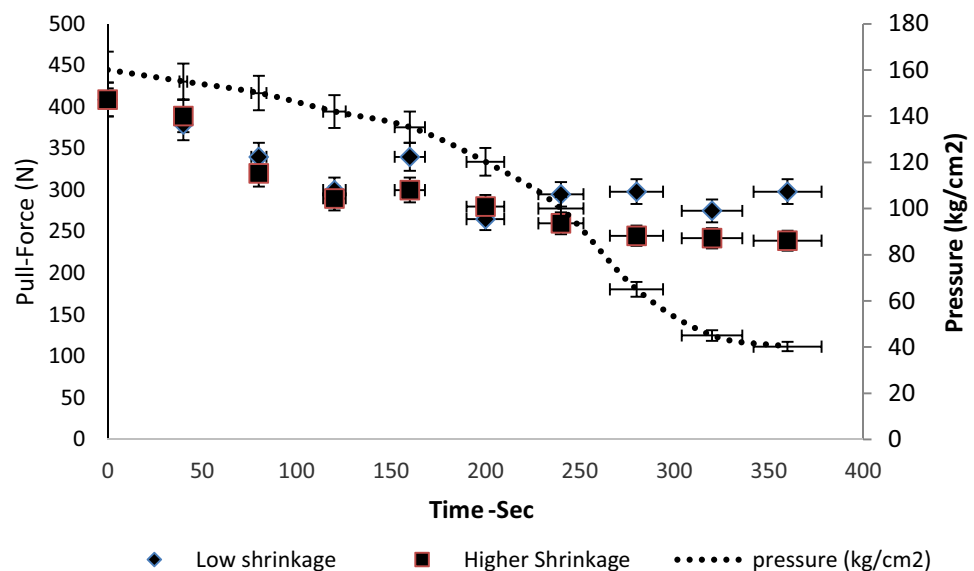
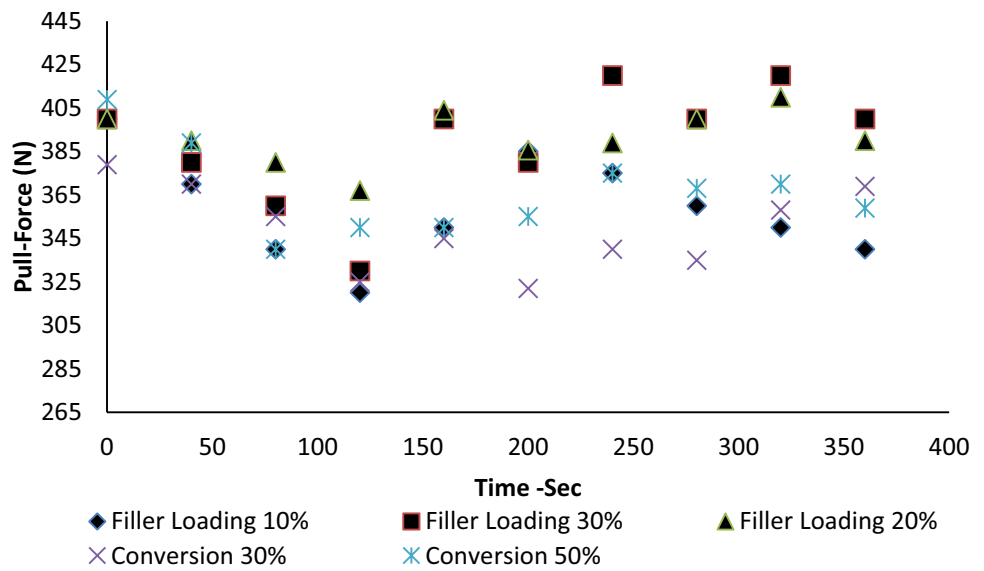
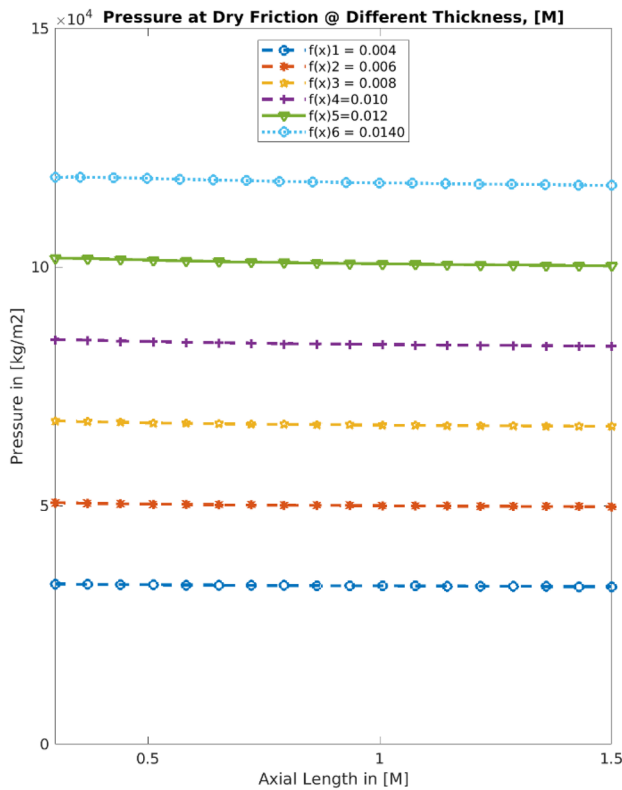


Fig. 16 Pull-force recorded using device during pulling post curing

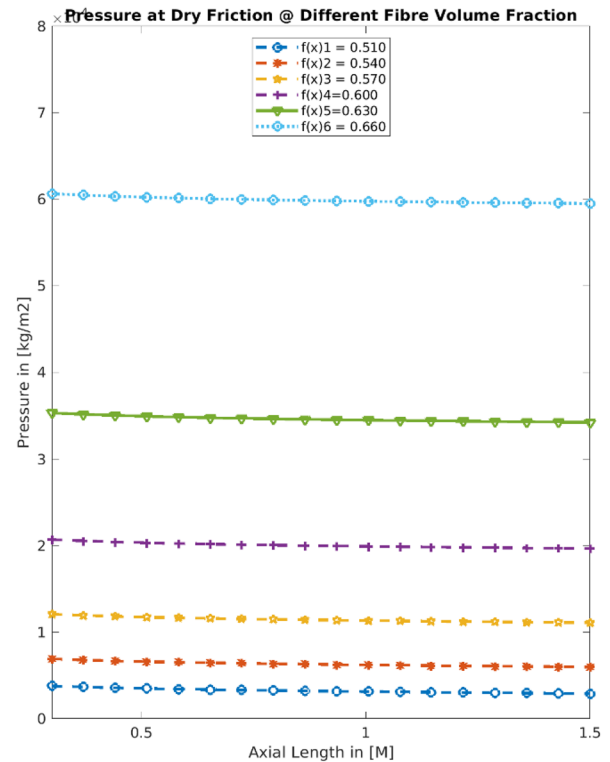


is much faster and abrupt at higher temperatures and after gelation, and the curing continues with much slower pace because of the restricted movement of reactive groups. It is worthy to mention that gelation effect at faster heating rate causes the reaction rate, i.e. a controlled diffusion. This

limited diffusion causes seldom failure to reach the complete conversion. Gelation time is accurately determined from half-life and the time required to reach the maximum cure rate as normally calculated by isothermal cure kinetics of unsaturated polyester resin.



(a)



(b)

Fig. 17 Influence of (a) fibre volume fraction and (b) profile thickness on compaction pressure during pulling

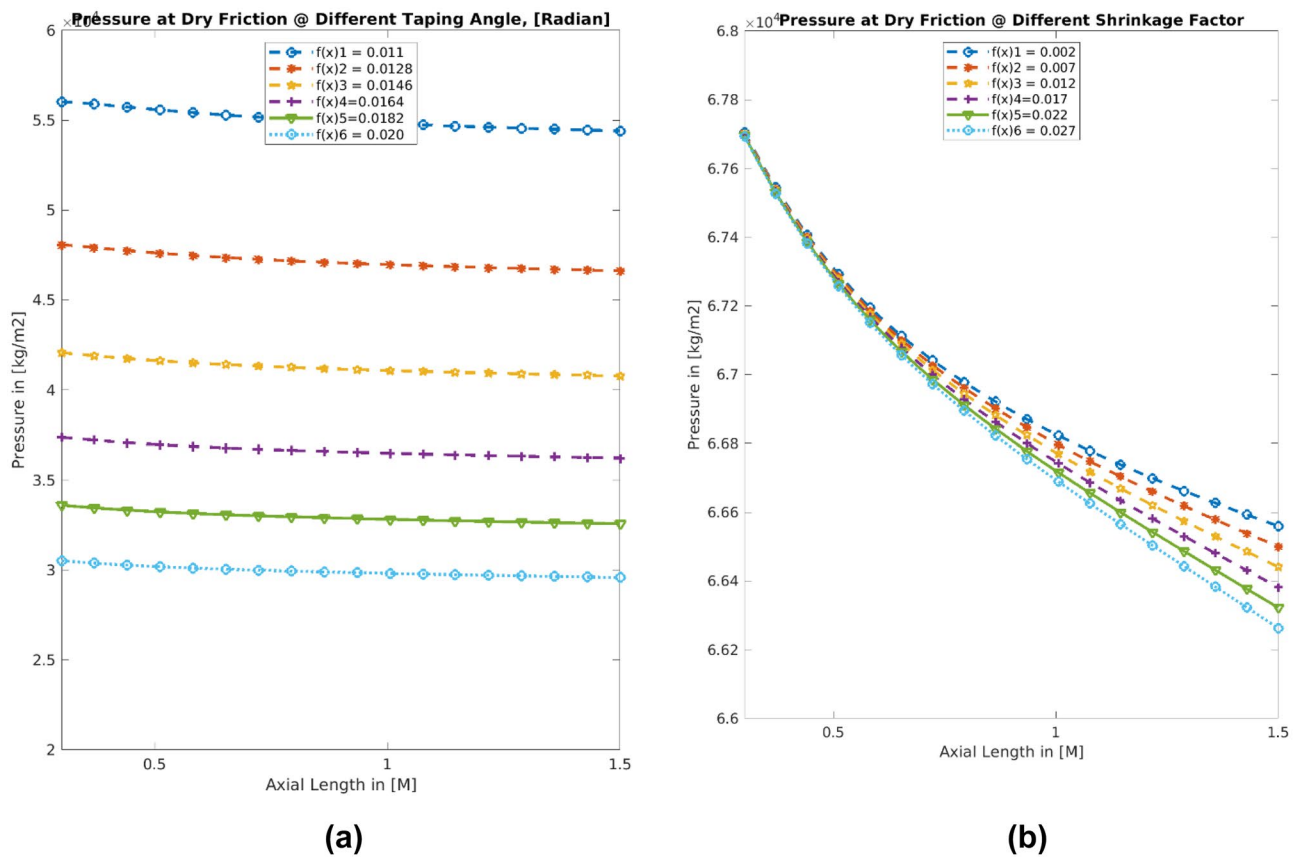


Fig. 18 Influence of pulling speed and tapping angle on pressure due to friction during pulling

3.6 Dynamic friction force after cure

Separately, using governing Eq. (45) as modified of Eqs. (43) and (44) and subsequent model fitting by using MATLAB was made to investigate post curing solid surface friction of product. In the governing equation, shrinkage-induced part detached is considered. In order to rule-out uncured fibre pack core of thick manufactured part, a parallel experiment of steel shim pulling, was conducted in short die length. The results recorded were not be in line with exactly with 2D plotted model fitting for solid surface friction. Experiment using the same short die with heated steel shim was also conducted to predict the pulling force beyond curing at profile at die surface. The device which has better control on speeds of pulling and temperature plate can have better accuracy to understand behaviour of pull force beyond curing. For this long-cured zone, pulling is mostly generated due to dynamic friction of composite in contact with die surface.

Dynamic dry friction on different resins with specific shrinkage factor during pulling was recorded at 105 °C as shown in Fig. 15. During the period of dry pulling, with initial drops, friction gets stabilised with time. In addition, it is observed, with time a steady state appeared at marginally

higher value of friction in the event of low shrinkage resin. Similarly, effect of filler and % conversion on friction during dry drag was studied as shown in Fig. 16, with initial drops, and friction embarks slow rising for all variants. The reason of initial drops is not clearly understood but increasing filler amount from 40% to the subsequent 30% and 10% shows incremental rising trend.

Beyond curing, comparatively higher cohesive force is expected between walls of the die and resin matrix at interface for low filler content resin which is an opposite condition for higher filler loading [38–45]. The initial drop may be explained as higher filler loading increase matrix morphology stiff and thereby reduces the dynamic frictional coefficient but with passing time, all variants get stabilised with higher friction at higher filler content [12, 13]. Further addition of filler makes the resin thicker, and rate of reaction slows down, and diffusion phenomena is more predominant and delayed conversion starts playing in due to heat on resin layer related to higher viscous resin-die interface ultimately decreasing stress compressibility.

Similarly, two different conversion of same resin was used to predict the behaviour of dynamic friction of the composite beyond curing. The reason of slightly higher

pull force for resin at higher conversion at start is not clearly understood. But apparently, higher molecular network restricts to slip initially [46, 47] but stimulate sliding on curing faster than resin at low conversion, reducing contact stress with time. Pulling force gets stabiles with time and difference between low and higher conversion is barely perceptible.

Unlike experiments pulling force in 2D plot sweeping time, axial length is sweep against pulling pressure. However, drops in pull-pressure are evident in resin with higher shrinkage factor due to increasing negative pressure on total pressure of solid friction. The paradigm of pressure drop is very steady, almost similar pattern and consistent as is observed in 2D-plot shown in Figs. 17a, b and 18a. As found for compaction and vicious, increase in tapping angle has negative influence on frictional pressure wherein thickness and fibre volume fraction and positive influence. The gradual and steady drop pressure with increasing resin shrinkage factor is perceptible on minimising scale of pressure axis as plotted in Fig. 18b. It can be concluded that increasing part thickness and fibre volume fraction increase pressure resolving from frictional loads. Amount of pressure goes up exponentially with increasing thickness and fibre volume fraction and wherein pressure drops are noticeable severe for change in shrinkage factor.

4 Conclusion

This study shows that for the pulling in open bath pultrusion, the pulling pressure for any cross-section encounters associated frictional force which gets influenced by many crucial parameters. This parameters include the die tapping angle, die radius, thickness and length of die, die surface smoothness, guiders and resin tank used, heater position from die entry, die temperature, pulling speed, fibre volume fraction, configuration of material at die interface, resin viscosity, resin releasing rate from reinforced fibre, size and porosity of filler and its loading percentage. Eventhough it is difficult to develop model which predicts paradigm of burgeoning pull-force during large-scale operation, the proposed modified mathematical equation enables one to comprehend effect of intricate process parameters on pull force measured and its fitting in the model. Pressure arises at compaction zone is always predominant over pressures like viscous drags and dynamic friction.

This study results show that during viscous phase, higher resin conversion leads to a higher friction. Unlike speed of pulling, viscous friction is much more significant when the low temperature (e.g. room temperature) wherein friction drops at higher temperature and eventually debilitate at

solidification. Again, it was found out that the die seizure/sloughing leads to fibre breakage. This is more prominent in case of smaller die due to surging adhesive force between die surface and resin, that can be mitigated by using mould releasing agents. Hence, sustainability of smooth operation during pulling relies on ultimate tensile strength of the part rather strength of the fibres being pulled in machine direction. On the other hand, gelling and post-curing solidification cause significant spikes in the pulling force on enlarging die length. However, longer dies in pultrusion benefits in maintaining good dimensional stability against heat distortion and therefore they should not be ruled out. Consequently, as observed in this study, it is worthwhile to mention that pull force measurement alone is not a satisfactory indicator of part curing at the exit and experimental verification on residence time, distribution heat and surface cure at the exit is required to substantiate at pulling operation.

Abbreviations ∇ : Pressure difference; V_f : Fibre volume fraction; k_c : Kozeny constant; P : Pressure normal to surface; V_a : Maximum fibre volume fraction; B : Transversal stiffness of fibres; dP/dx : Change of pressure difference with change in axial distance; V_{fx} : Fibre volume fraction as functions; x : Axil distance; F_{tot} : Total force; w : Die width; \dot{p} : Resin injection pressure; σ : Contact pressure; δ : Fibre deflection; L : Length of the fibre segment; l_0 : Initial height of the prism; \dot{w} : Width of the prism; l : Height of the prism; f : Co-efficient of friction; h_L : Height of flat portion of the conical die from centre; A : None; Φ : Porosity; L_w : Linear weight of fibre; U_x : Resin flow speed; $Q(x)$: Volumetric flux; η_a : Apparent viscosity; γ : Shear rate; n : Dimensionless constant; θ : Initial taping angles; P_c : Pressure at compaction; P_v : Pressure due to viscosity; η_a : Apparent viscosity; η_v : Average viscosity; $\hat{\theta}$: Contact angle of liquid–solid phase; P_{ef} : Effective pressure due to dry friction; δR : Shrinkage of part; K : Permeability; R : Particle radius; β : Constant representing ratio of span length to span height of the fibres involved.; V_0 : Initial fibre volume; U : Pulling speed; $K_{(x)}$: Longitudinal permeability; $\Delta v/v$: Resin resultant volume changes due to thermal expansion and overall shrinkage; $P(x)$: Pressure at specific axial distance; F_{com} : Force due to compression; F_{vis} : Viscous force; F_{fric} : Force due to frition; τ : Shear strength/stress; F : Contact force of the fibres; E : Modulus of the fibres; I : Inertia of bending of the fibres; l_{min} : Minimal height; G : Theoretical bulk modulus; d : Diameter of the fibre; L_m : Length o taper section; ρ_f : Density of fibres; N_r : Number of roving in specific volume; δP : Pressure gradient; $h(x)$: None; $Q_R(x)$: Relative matrix flux; η_0 : Initial viscosity; λ : Resin layer thickness; G : Shape factor; P_d : Pressure due to drag; P_f : Pressure due to dry friction; $h_{(x)}$: Height of conical die at x ; r : Distance between the layers or fibres; A_d : Adhesion load; θ_f : Average angle; S : Shrinkage factor; λ : Time constant

Author contribution AM: conceptualization, investigation, methodology, writing – original draft, writing – review and editing, validation, funding acquisition. JN: conceptualization, methodology, writing – review and editing, project administration, resources, funding acquisition supervision.

Funding The authors are thankful to financial support for AM from Shapoorji Pallonji Group through secondment to Robert Gordon University for a Research Fellowship in a project titled ‘Honeycomb Composite Structures for Ballistic Protection’ Project No. 120437.

Availability of data and material The image data used will be provided on request.

Code availability The code used will be provided on request.

Declarations

Consent to participate N/A.

Consent for publication N/A.

Conflict of interest The authors declare no competing interests.

Open Access This article is licensed under a Creative Commons Attribution 4.0 International License, which permits use, sharing, adaptation, distribution and reproduction in any medium or format, as long as you give appropriate credit to the original author(s) and the source, provide a link to the Creative Commons licence, and indicate if changes were made. The images or other third party material in this article are included in the article's Creative Commons licence, unless indicated otherwise in a credit line to the material. If material is not included in the article's Creative Commons licence and your intended use is not permitted by statutory regulation or exceeds the permitted use, you will need to obtain permission directly from the copyright holder. To view a copy of this licence, visit <http://creativecommons.org/licenses/by/4.0/>.

References

- Baran I, Tutum CC, Hattel JH (2013) The effect of thermal contact resistance on the thermosetting pultrusion process. *Composites B* 95:995–1000
- Batch GL, Macosko CW (1990) Analysis of pressure, pulling force, and sloughing in pultrusion. American Society of Mechanical Engineers, Heat Transfer Division, (Publication) HTD 132:109–112
- Struzziero G, Maistros GM, Hartley J, Skordos AA (2021) Materials modelling and process simulation of the pultrusion of curved parts G. *Composites Part A* 144:106328
- Baran I, Tutum CC, Nielsen MW, Hattel JH (2013) Process induced residual stresses and distortions in pultrusion. *Composites B* 51:148–161
- Dong C (2009) Modeling the process-induced dimensional variations of general curved composite components and assemblies. *Composites A* 40(8):1210–1216
- Gorthala R, Roux JA, Vaughan JG (1994) A model to predict resin pressure/back flow in the tapered inlet of a pultrusion die. *J Reinf Plast Compos* 13
- Rahatekar SS (2005) Injection pultrusion simulation for polyester/glass mat/rovings/mat composites. *J Reinf Plast Compos* 24(1):53–68
- Astrom BT (1993) Modeling approach to thermoplastic pultrusion. I: Formulation of models. *Polym Compos* 14:3
- Baran I, Hattel JH, Akkerman R, Tutum CC (2015) Mechanical modelling of pultrusion process. *Appl Compos Mater* 22(1):99–118
- Vernet N et al (2014) Experimental determination of the permeability of engineering textiles: benchmark II. *Compos A Appl Sci Manuf* 61:172–184
- Lackey E, Vaughan JG (1994) An analysis of factors affecting pull force for the pultrusion of graphite/epoxy composites. *J Reinf Plast Compos* 13(3):188–198
- Mukherji A, Tarapore N, Njuguna J (2022) Determination of cure mechanism inside die for a part manufacturing during large-scale pultrusion. *J Appl Polym Sci* 139(17):52035
- Mukherji A, Njuguna J (2021) Shock propagation behaviour and determination of Gruneisen state of equation for pultruded polyester/glass fibre-reinforced composites. *Compos Struct* 262:113444
- Josiasvd W, Prieur J, Du P (1994) Quantification of unidirectional fiber bed permeability. *J Compos Mater* 28(7):619–637
- Bates PJ, Taylor D, Cunningham M (2000) Transverse permeability of direct glass rovings. *J Reinf Plast Compos* 19(15):1217–1226
- Gutowski TG, Dillon G (1992) The elastic deformation of lubricated carbon fiber bundles: comparison of theory and experiments. *J Compos Mater* 26(16):2330–2347
- Gutowski T, Dahmus J, Thiriez A (2006, May) Electrical energy requirements for manufacturing processes. In: 13th CIRP international conference on life cycle engineering, vol 31, no 1. Leuven, Belgium, pp 623–638
- Arindam M (2017) Prediction of cure mechanism of polyester resin based composites across die during pultrusion process. 4th Annual National conference. 6th Recent Advancement on Polymer Technology. National conformance Jan 27–28th India
- Arindam M, Patil K, Tarapore ND, Wakure G (2017) Material configuration in the die, influences pultrusion process parameters and part properties. 6th Recent Advancement on Polymer Technology. National conformance Jan 27–28th, India
- Arindam M, Patil S (2017) Flow behaviour of Ferro fluids and its effect on thermal conductivity. 6th Recent Advancement on Polymer Technology. National conformance Jan 27–28th, India
- Arindam M, James N (2018) Material configuration in the die, influences pultrusion process parameters and part properties. 4th International Conference on Structural Nano Composites (NANO-STRUC2018). 23–25th May, Berlin, Germany
- Kim DH, Han P-G, Jin GH, Lee WI (1997) A model for thermosetting composite pultrusion process. *J Compos Mater* 31(20):2105–2122
- Joshi S, Lam Y (2006) Integrated approach for modelling cure and crystallization kinetics of different polymers in 3D pultrusion simulation. *J Mater Process Technol* 174(1–3):178–182
- Baran I, Akkerman R, Hattel JH (2014) Modelling the pultrusion process of an industrial L-shaped composite profile. *Compos Struct* 118:37–48
- Carlone P, Palazzo G, Pasquino R (2006) Pultrusion manufacturing process development by computational modelling and methods. *Math Comput Model* 44(7–8):701–709
- Baran I, Hattel JH, Tutum CC, Akkerman R (2015) Pultrusion of a vertical axis wind turbine blade. Part-II International Journal of Material Forming 8(3):367–378
- Carlone P, Baran I, Hattel JH, Palazzo GS (2013) Computational approaches for modeling the multiphysics in pultrusion process. *Adv Mech Eng* 5(0):301875
- Baran I, Hattel JH, Akkerman R (2015) Investigation of process induced warpage for pultrusion of a rectangular hollow profile. *Compos B Eng* 68:365–374
- Deng HY, Wang ZQ, Wei T (2016) Study on grouting di_usion theory based on rheology of CW epoxy slurry.J. Yangtze River Sci Res Inst 33:121–124
- Cheng PD (2011) Study on flow characteristics of viscous time-varying grouting slurry in porous formation.Ph.D. Thesis, Shanghai University, Shanghai, China
- Zhu XD, Wang LJ (2017) Analysis of rheological properties and curing properties of RTM Epoxy Resin. *Fiber Reinf Plast Compos* 8:97–101
- Liu ZF, Xiao JY, Zeng JC (2008) Study on the process performance of low viscosity epoxy resin VIM. *J Natl Univ Def Technol* 30:20–24
- Halley PJ, Mackay ME (1996) Chemorheology of thermosets: an overview. *Polym Eng Sci* 36:593–609

34. Kiuna N, Lawrence CJ (2002) A model for resin viscosity during cure in the resin transfer moulding process. *Compos Part A* 33:1497–1503
35. Zhang W, Duan YX, Zhao Y (2000) Study on low viscosity epoxy resin system for resin transfer moulding process. *Polym Mater Sci Eng* 2000(16):86–88
36. Renato MB (2017) Modelling and simulation of the closed injection pultrusion process. Dissertation of M.Sc. Karlsruher Institut für Technologie (KIT)
37. Zhenhua S, Zaiqin W, Da Z, Tao W (2019) Study on rheological behavior and surface properties of epoxy resin chemical grouting material considering time variation. *Materials* 12:3277
38. Chang WR, Etsion I, Bogy DB (1988) Static friction coefficient model for metallic rough surfaces. *J Tribol* 110:57
39. Chang WR, Etsion I, Bogy DB (1987) Elastic-plastic model for the contact of rough surfaces. *ASME J Tribol* 109:257–263
40. Tian QL, Peng F, Yuwei W, Shuxin L, Xinmiao M (2021) Developing an innovative curved-pultruded large-scale GFRP arch beam. *Compos Struct* 01:256
41. Mukherji A, Tarapore ND, Wakure GN (2016) Designing of hybrid structured glass laminated transparent nano composites through vacuum infusion technique. *MST Int J Chem* 1:1
42. Chang WR, Etsion I, Bogy DB (1988) Adhesion model for metallic rough surfaces. *ASME J Tribol* 50–56
43. Berger GR, Steffel C, Friesenbichler W (2015) On the use of interfacial tension parameter to predict reduction of friction by mold coatings in injection molding of polyamide 6. *Proceedings of the Regional Conference Graz – Polymer Processing Society PPS*
44. Berger GR, Steffel C, Friesenbichler W (2015) A study on the role of wetting parameters on friction in injection molding. Submitted to special issue on PMI: polymers and moulds innovations. *Int J Mater Prod Technol (Indersci Publ)*
45. Delaney KD, Bissacco G et al (2012) A structured review and classification of demolding issues and proven solutions. *Int Polym Proc* 27(1):77–90
46. Kirill M, Alexander V, Alexander S, Iskander A (2021) Thermo-plastic pultrusion: a review polymers 13:180
47. Steffel C (2014) Studies on the predictability of friction between polymers and coated/uncoated mold surfaces by wetting parameters. Master thesis, Montanuniversitaet Leoben

Publisher's note Springer Nature remains neutral with regard to jurisdictional claims in published maps and institutional affiliations.